Design and Comparison of Two Control Strategies for Multi-DOF Articulated Robotic Arm Manipulator

Raza ul Islam[*,], Jamshed Iqbal[*], Qudrat Khan[**]**

[*]*Department of Electrical Engineering,*
COMSATS Institute of Information Technology, Islamabad, Pakistan
[**]*Center for Advance Studies in Telecommunication (CAST),*
COMSATS Institute of Information Technology, Islamabad, Pakistan
E-mail: m.razaulislam@yahoo.com, jamshed.iqbal@comsats.edu.pk, qudratullah@comsats.edu.pk

Abstract: This paper is aimed at mathematical modeling and design of a robust control strategy for a multi Degree Of Freedom (DOF) manipulator. A novel AUTonomous Articulated Robotic Educational Platform (AUTAREP), centered on a 6 DOF arm, is introduced in the research. Kinematic and dynamic models of the robotic arm have been derived. The kinematic model has been validated through simulation as well as experimentations on a prototype while the dynamic model has been demonstrated through mathematical formulation. Based on the system dynamics, Sliding Mode Controller (SMC) for the arm has been designed and tested for various trajectories to characterize its response. The tracking performance of the controller is then compared with another non-linear control strategy Computed Torque Control (CTC). Based on various performance indices, simulation results demonstrate superior performance of SMC over its CTC counterpart.

Keywords: Robot control, Nonlinear control, Robust control, Dynamic modeling, Robot kinematics, Educational platform

1. INTRODUCTION

The history of robotics dates back to midst of 17th century when a human-sized mechanical doll was developed. Since then, research in robotics has been evolving gradually. At present, robots are being extensively employed in industries like medical, automotive, defense and other fields owing to the revolution in technology and advancements in areas like control, modeling, mechanism design, mechanics, Artificial Intelligence (AI) and neural networks. Diverse kind of robotic manipulators have been realized for numerous applications including assembling, inspection, material processing, loading/unloading, semiconductor wafer etching etc.

Performance of a robotic manipulator is characterized by its well-defined control strategy. The overall control problem consists of derivation of kinematics and dynamics of a manipulator followed by the control design to achieve desired system response. In fact, the precision, stability, repeatability and through put of a robotic arm can only be obtained with a sophisticated control law. Associated key challenges include handling of the system complexity and catering for the dynamic nature of environment and required tasks.

Both classical and robust techniques are practiced to control a robot manipulator. Considering the classical approach, a Proportional Integral Derivative (PID) controller implementation on real robots including a mobile robot (Iqbal *et al.,* 2013) and a multi-Degree Of Freedom (DOF) serial link exoskeleton robot (Iqbal *et al.,* 2010, 2011) has been reported. The significance of PID approach in industrial robotic manipulators has been presented in (Antonio *et al.,* 2011). This design proposed a nonlinear PID controller with bounded torques, ensuring global asymptotic stability. Combining classical control techniques with modern control approaches results in an improved transient response in uncertain circumstances (Ouyang *et al.,* 2014; Birla and Swarup, 2013). Work in (Farzin *et al.,* 2012a) has combined Computed Torque Control (CTC) with PD and PID. Based on CTC, (Duy *et al.,* 2008) have presented a comparison between Locally Weighted Projection Regression (LWPR) and Gaussian Process Regression (GPR).A Passivity Based Control (PBC) technique following a direct adaptation law to improve the response against model uncertainties and disturbances has been proposed in (Nawal and Lamir, 2011). Researchers have proposed PBC for antagonistic bi-articular muscles (Hiroyuki *et al.,* 2011) and obstacle avoidance for robot manipulators (Khoi and Robert, 2005). Work in (Jingmei *et al.,* 2012) has attempted to improve trajectory precision and performance of robotic manipulators by combining Variable Structure Compensator (VSC), PID and an adaptive fast method. Chattering phenomenon is also reduced with increased system response time. (Suolin *et al.,* 2010) reports a feed-forward control with VSC, improving tracking precision and dynamic performance. A chattering free VSC controller using the adaptive gains to approximate unknown system parameters has been presented in (Dimitri and Anwari, 2009). A Sliding Mode Control (SMC) based onintegral sliding surface and adaptive switching function to estimate the uncertainty in system parameters has been mentioned in (Jing *et al.,* 2011). The results have shown deceased uncertainty and reduced system chattering using low controller gains. Work in (Farzin *et al.,* 2012b) simulates SMC based control of Programmable Universal Manipulation

Arm (PUMA) 560 robotic manipulator. (Wen-Hua et al., 2000) have proposed a Nonlinear Disturbance Observer (NDO) based control dependent on maximum velocity and physical parameters. The global exponential stability is guaranteed for the proposed system. The control formulation finds its application in sensor less torque control, independent joint control, friction compensation and fault diagnosis. Another Disturbance Observer Based controller (DOBC) has been presented in (Chia-shang and Peng, 2011) to eliminate major external disturbances by incorporating a Lyapunov-based feedback estimation law. The feed forward correction term further improves the estimation.

Despite a long history of controller designs for robots, the modern control systems for multi-DOF manipulators have the capacity to be enriched further. The present work is related with robust control of a 6-DOFrobotic arm, on which AUTonomous Articulated Robotic Educational Platform (AUTAREP) is centered. Figure 1 illustrates AUTAREP while Table 1 lists its main features.

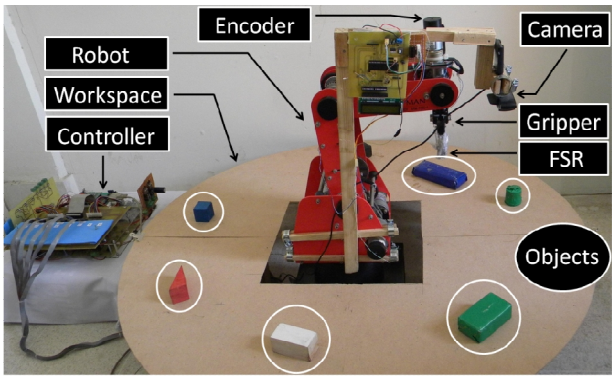

Fig. 1. AUTAREP: A platform with distinguishing capabilities to test and analyze performance of control algorithms.

Table 1. AUTAREP specifications.

Parameters	Specs.	Description
Kinematics	No. of joints	5
	No. of DOF	6
	Range Of Motion (ROM)	Wrist Pitch: 260° Wrist Roll: 360° Elbow: 172° Shoulder: 90° Waist: 310°
Physical	Locomotion	Articulated links
	Actuation	6 DC Servo motors
	Weight	33 Kg
	Dimensions	Base: ϕ220X180(H) mm
		Arm length: 220+220 mm
Sensing	Vision	Camera (Logitech)
	Force	FSR attached at Gripper
	Position	Optical encoders
Performance	Position precision	±1.5mm
	Repeatability	± 1mm
	Movement speed	100mm/s (max.)
	Payload	1 Kg
	Action radius	580mm (largest)

This paper is structured as follows: Section 2 addresses review of control strategies for robotic manipulators; The derived mathematical models of the robotic manipulator are presented in Section 3; Section 4 introduces controller design based on the derived models; Results are presented in Section 5. Finally Section 6 comments on conclusion and future work.

2. REVIEW OF CONTROL STRATEGIES FOR MANIPULATORS

Control systems have always been studied in technological research communities. Going beyond linear control algorithms (e.g. PID), various robust and adaptive control strategies to cope with non-linearity and uncertain behaviour of robotic manipulators have been reported. Such control strategies include Feedback linearization, VSC, PBC, DOBC etc.

Feedback linearization is an approach to transform a nonlinear system into an equivalent linear system by cancelling its nonlinear dynamics. Exact values of parameters along with states values are required for this transformation. There are two main types of Feedback linearization: Output linearization and Input/State linearization. In the first type, the output is differentiated until the input appears while in the second type, a new output is defined so that the relative degree becomes same as that of the system order. A special case of feedback linearization is CTC which utilizes both nonlinear feedback and linear control techniques. In Feedback linearization, a close loop Linear Time Invariant (LTI) system is obtained assuring global asymptotic stability.

In VSC (also termed as Sliding Mode Control), the imprecision and uncertainties are modelled first and then the response of system is stabilized using nonlinear feedback. In this particular approach, initially the error is derived onto the switching surface which has invariance to model uncertainties and disturbances. After this, sliding mode is initialized. The trajectories that are brought onto the sliding manifold where they stay independent of the model uncertainties.

Passive systems do not produce energy. PBC is based on physical passive structure of the robotic system. The origin of the passive system is stable. The system is stabilized by incorporating the feedback that forces the system to become passive despite of uncertainties in parameters and nonlinearities.

Another technique for controlling a robotic manipulator is DOBC which approximates the sum of the disturbance torques. First the difference between output of the nominal model and actual output is computed. An equivalent disturbance is then applied to the nominal model. Moreover, the above discussed control strategies can be used together with DOBC to improve performance of a system. In DOBC an independent nominal model controller for a multi-link robotic system can be designed by considering the coupling torques as unknown external torques, so as to control the joints independently.

An in-depth comparative review, mentioning salient features and associated challenges of each control strategy has been presented in (Fayaz *et al.,* 2012)

3. MODELING ROBOTIC MANIPULATOR

In correspondence with the human arm, the robotic manipulator in the present work consists of five revolute joints from waist to wrist. The manipulator is equipped with a two-fingered gripper for object manipulation. Such an arm with wide range of capabilities is intensively used for research, teaching and training purpose in academic and industrial environments. Figure 2 illustrates the arm configuration.

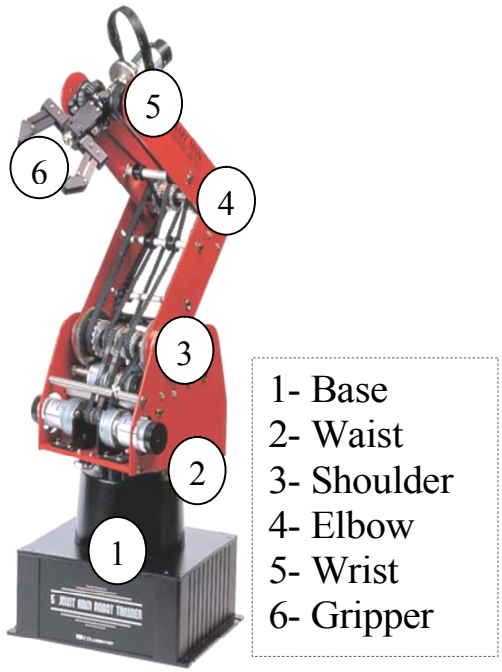

Fig.2. Arm joints configuration.

The specifications mentioned in Table 1 have been used in robot analysis prior to design of the control strategies. Both kinematic and dynamic models of the arm have been derived. Kinematic model includes derivation of solution of Forward as well as Inverse problem.

3.1 Forward Kinematic (FK) model

The study of FK of a robot can be carried out by different methods. Two commonly used methods are based on Denavit-Hartenberg (DH) parameters and successive screw displacements. Also geometric methods are frequently used by some researchers for serial manipulators of simple geometry. In the present work, DH method has been used to develop the kinematics because of its versatility and acceptability for modelling of any number of joints and links of a serial manipulator regardless of complexity. Figure 3 shows the kinematic representation of the arm. Frame assignment and derivation of DH parameters are presented in (Raza *et al.,* 2012). Table 2 lists these parameters.

Table 2. DH parameters of robotic arm.

Parameter	Symbol	Joint (*i*)					
		1	**2**	**3**	**4**	**5**	**6**
Link twist	α_{i-1}	0	-90°	0	0	-90°	0
Link length	a_{i-1}	0	0	l_2	l_3	0	0
Joint distance	d_i	l_1	0	0	0	0	l_4
Joint angle	θ_i	θ_1	θ_2	θ_3	θ_4	θ_5	0

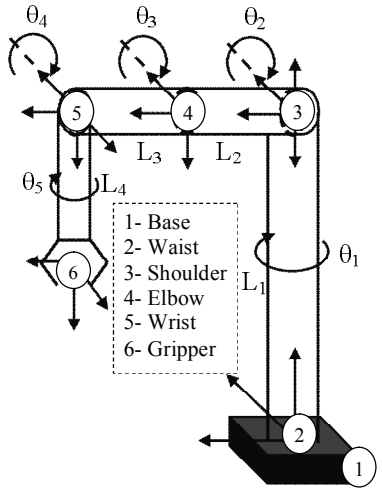

Fig.3. Robot mechanism.

Considering the following nomenclature,

$$c_{ab} = \cos(a+b) = c_a c_b - s_a s_b$$

$$c_{abc} = \cos(a+b+c)$$

The overall rotation and translation matrices indicating end-effector (frame {6}) into base (frame {0}) is given by (1) and (2) respectively.

$$ {}^{0}_{6}Rot = \begin{bmatrix} c_1 c_{234} c_5 + s_1 s_5 & -c_1 c_{234} s_5 + s_1 c_5 & -c_1 s_{234} \\ s_1 c_{234} c_5 - c_1 s_5 & -s_1 c_{234} s_5 - c_1 c_5 & -s_1 s_{234} \\ -s_{234} c_5 & s_{234} s_5 & -c_{234} \end{bmatrix} \quad (1)$$

$$ {}^{0}_{6}Trans = \begin{bmatrix} c_1 A \\ s_1 A \\ B \end{bmatrix} \quad (2)$$

Where

$$A = -l_4 s_{234} + l_3 c_{23} + l_2 c_2$$

$$B = l_1 - l_4 c_{234} - l_3 s_{23} - l_2 s_2$$

Combining (1) and (2) resulted in Homogeneous Transformation matrix given in (3) which represents the kinematic model of the robotic arm.

$$ {}^{0}_{6}T = \begin{bmatrix} c_1 c_{234} c_5 + s_1 s_5 & -c_1 c_{234} s_5 + s_1 c_5 & -c_1 s_{234} & c_1 A \\ s_1 c_{234} c_5 - c_1 s_5 & -s_1 c_{234} s_5 - c_1 c_5 & -s_1 s_{234} & s_1 A \\ -s_{234} c_5 & s_{234} s_5 & -c_{234} & B \\ 0 & 0 & 0 & 1 \end{bmatrix} \quad (3)$$

3.2 Inverse Kinematic (IK) model

Given the desired position and orientation coordinates (pose)

of the end-effector, IK Model computes the corresponding joint angles. Closed form approach (Algebraic and Geometric methods) has been used to derive the IK model for the arm. The orientation of gripper has been realized geometrically while the closed form equations for each joint angle of the robotic arm have been derived algebraically (4-7).

$$\theta_1 = Atan2(p_y, p_x) \tag{4}$$

The orientation of the gripper w.r.t. base is θ_{234} as can be seen in Fig. 4. For an IK problem, this orientation is known. The optimum orientation for a gripper to manipulate an object can be obtained by designing a performance matrix based on results of captured images.

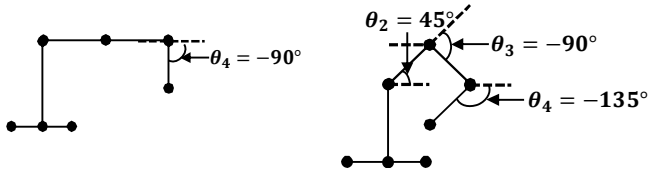

(a) (b)

Fig. 4. Angles involved in orientation: (a) Robot at home position (b) Varying angles to shift the wrist.

The remaining joint angles are computed as follows (Iqbal et al., 2013b)

$$c_3 = \frac{(c_1 p_x + s_1 p_y + l_4 s_{234})^2 + (p_z - l_1 + l_4 c_{234})^2 - {l_2}^2 - {l_3}^2}{2 l_2 l_3}$$

$$s_3 = \pm\sqrt{1 - {c_3}^2}$$

$$\theta_3 = Atan2(s_3, c_3) \tag{5}$$

$$c_2 = \frac{(c_1 p_x + s_1 p_y + l_4 s_{234})(c_3 l_3 + l_2) - (p_z - l_1 + l_4 c_{234}) s_3 l_3}{(c_3 l_3 + l_2)^2 + {s_3}^2 {l_3}^2}$$

$$s_2 = -\frac{(c_1 p_x + s_1 p_y + l_4 s_{234}) s_3 l_3 + (p_z - l_1 + l_4 c_{234})(c_3 l_3 + l_2)}{(c_3 l_3 + l_2)^2 + {s_3}^2 {l_3}^2}$$

$$\theta_2 = Atan2(s_2, c_2) \tag{6}$$

$$\theta_4 = \theta_{234} - (\theta_2 + \theta_3) \tag{7}$$

The derived model has been validated by simulation as well as through implementation on the physical prototype.

(i) Software based validation

Based on the user-defined desired pose, the developed IK model computes the corresponding joint angles. These angles are verified using MATLAB© where FK model gives resultant pose. Matching these with the original user-defined coordinates validates the IK model. The validation cycle is illustrated in Fig. 5.

Example: Considering user-defined coordinates as x= 230mm, y= 50mm, z= 250mm. Corresponding to these coordinates, developed IK model resulted in joint angles:

θ_1= 12.2648°, θ_2=-44.5373°, θ_3= 89.3551°, θ_4=-14.8178°

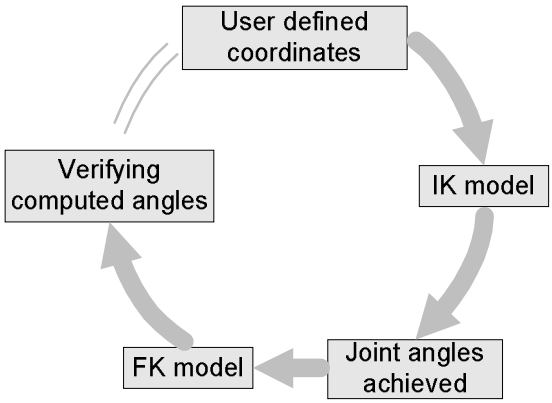

Fig.5. Software based validation process.

These angles of various joints of the robotic arm (Fig. 6), when fed to FK model in the MATLAB Tool Box for Robotics, resulted in homogeneous transformation matrix as:

$$T = \begin{bmatrix} 0.8463 & 0.2124 & -0.4886 & 230.0000 \\ 0.1840 & -0.9772 & -0.1062 & 50.0000 \\ -0.5000 & -0.0000 & -0.8660 & 250.0000 \\ 0 & 0 & 0 & 1.0000 \end{bmatrix}$$

The coordinates in the last column, indicating position of end-effector w.r.t. base, are exactly same as the given input. This witness that angles computed by IK model are correct, thus validating the model.

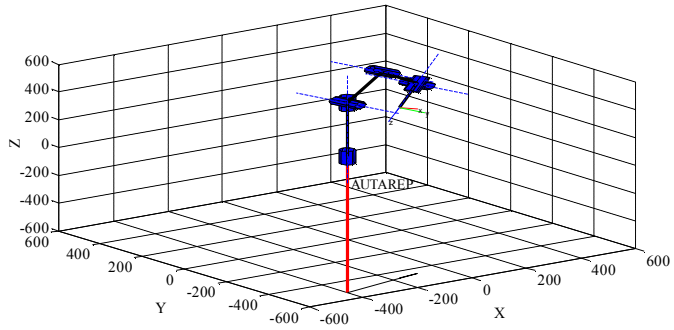

Fig. 6. Joint configuration in example.

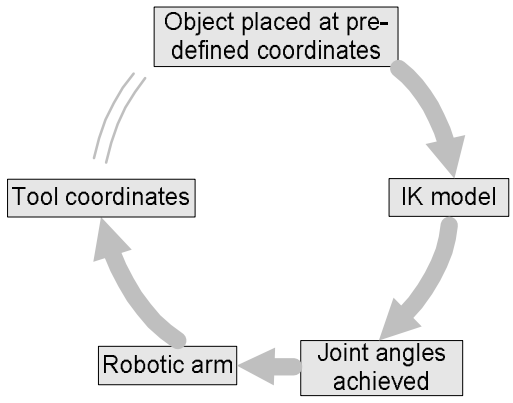

Fig. 7. Hardware based validation process.

(ii) Hardware based validation

Going one step forward, the derived IK model has been validated using real robotic arm. An object (e.g. key chain) is placed at known position. The developed IK model computes the required joint angles in correspondence with the object coordinates. These joint angles, after mapping in encoder ticks are commanded to the robotic arm. If the robot moves to the pre-defined object coordinates, this is an indication that the input angles (and thus derived IK model) are correct. Figure 7 illustrates the cycle of hardware validation.

Example: The hardware validation has been demonstrated by implementing 'pick and place' task where both the source and destination positions are known. Based on these coordinates, the derived IK model computes the required joint angles for source as well as destination positions. Driven by these angles, the robotic arm thus first moves to the source location (Fig. 8a), picks the object (Fig. 8b) and then finds its way to the destination (Fig. 8c) finally placing the object at destination (Fig. 8d).

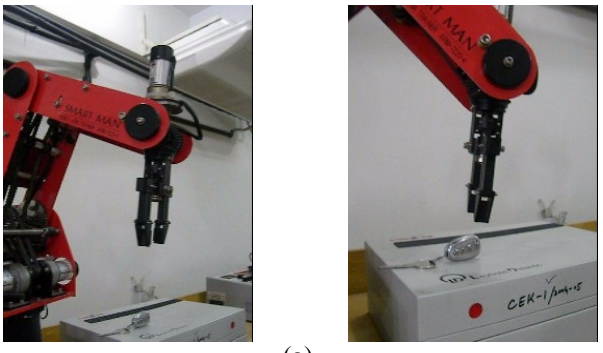

(a)

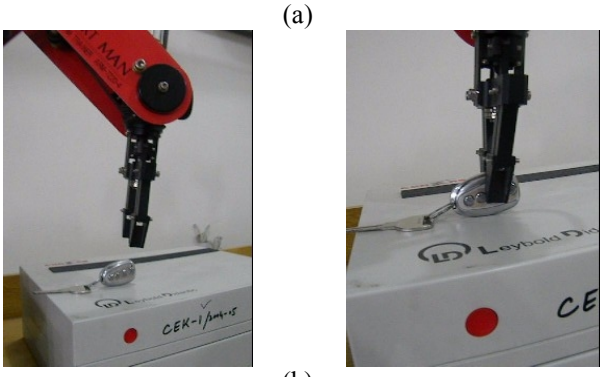

(b)

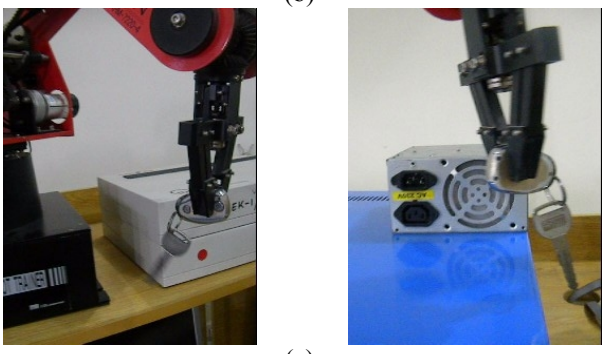

(c)

(d)

Fig. 8. Pick and place task (a) Moving to source (b) Picking the object (c) Moving to destination (d) Placing the object.

3.3 Dynamic model

Dynamics is concerned with the analysis of forces and torques acting on a body due to acceleration and deceleration. (Groover *et al.,* 2008). Primarily intended for simulation of robot motion, dynamics is investigated to devise control strategy and to evaluate kinematic design. In forward dynamics, the system response is determined for defined torques while in inverse dynamics, actuator torques are computed for specified trajectories.

In the present work, the dynamic model of the robotic arm has been derived using Eular-Lagrange approach. It is an energy based formulation (Saha, 2008) which is most commonly used because of its relatively simple and compact description.

Table 3 mentions nomenclature for deriving dynamic model of the robotic arm.

Table 3. Nomenclature for dynamic model.

Symbol	Description
m_i	Mass of link *i*
v_{c_i}	Linear velocity of link *i* w.r.t Centre of Mass
${}^i_i\omega$	Angular velocity of link *i* w.r.t. its frame *i*
${}^i_iI$	Inertia tensor of link *i* w.r.t. its frame *i*
${}^c_iP$	Position of Centre of Mass of link *i*
k_T	Total kinetic energy related to each link
u_T	Total potential energy related to each link
u_{refi}	Reference potential energy

The Kinetic and Potential energies of each link of the arm have been computed using (8-9) respectively.

$$k_i = \frac{1}{2} m_i v_{c_i}^T v_{c_i} + \frac{1}{2} {}^i_i\omega^T {}^i_iI {}^i_i\omega \quad (8)$$

$$u_i = -m_i g^T {}^c_iP + u_{refi} \quad (9)$$

Lagrangian (10) has been computed by difference of Kinetic and Potential energies of complete system (Craig *et al.,* 2005). Torque for each link is then computed by differentiating Lagrangian w.r.t θ and $\dot{\theta}$ as given by (11).

$$L = k_T - u_T \quad (10)$$

$$\tau = \frac{d}{dt}\frac{\partial L}{\partial \dot{\theta}} - \frac{\partial L}{\partial \theta} \quad (11)$$

The resulting torque equation of Dynamic model can be represented in joint space form as

$$\tau = M(q)\ddot{q} + V(q, \dot{q}) + G(q) \quad (12)$$

τ is representing the joint torque, $M(q)$ is the inertia tensor, $V(q, \dot{q})$ is composed of Centrifugal and Corollis forces, $G(q)$ matrix represents gravity. The derived model has been given in appendix A.

The dynamic model has been verified by using the Inertia matrix property of being semi-positive definite as highlighted in (M. Fayaz *et al.,* 2012) i.e. $V^T*M*V>0$. The joint trajectories are shown in Fig. 9(a) while the corresponding positive definite condition is depicted in Fig. 9(b).

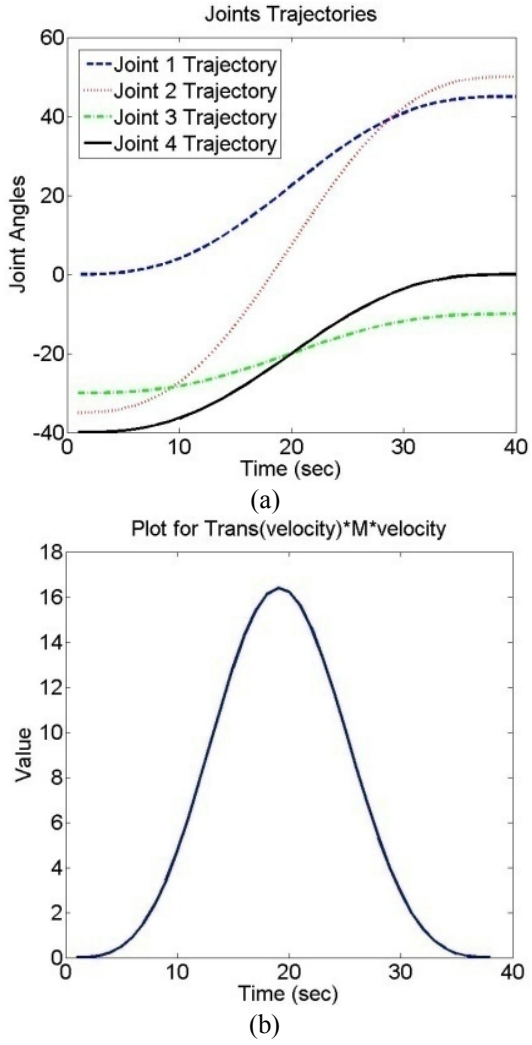

Fig.9. Dynamics validation (a) A set of joint trajectories (b) Positive definite condition.

Given the joint trajectories of Fig. 9a, the dynamic model of the robotic arm gives the required joint torques shown in Fig. 10.

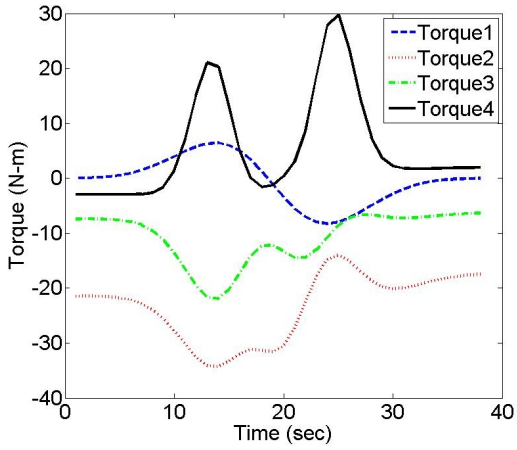

Fig. 10. Joints torque required to execute trajectories of Figure 9a.

4. CONTROLLER DESIGN

The control problem, in general, consists of (i) derivation of dynamic models of the manipulator (Section 3) (ii) using these models to design control strategies to acquire required performance (Fu et al., 2008).

The first control strategy under consideration in this research is CTC. The main advantage of this technique is its potentially higher tracking accuracy, lower feedback gains, higher suitability for compliant control and lower energy consumption etc. CTC utilizes the idea of Feedback linearization and offers availability of number of linear control techniques. Figure 11illustrates CTC implementation. Two controllers are shown here. Controller 1, working in inner loop as a compensator, linearizes the system. This loop has been designed based on non-linear dynamics of the robotic manipulator. Controller 2, working in the outer loop, implements a linear control technique (PD or PID) to achieve the desired response. The goal is to ensure that the manipulator follows the desired trajectory. So, controller 2 reduces the tracking error defined by (13).

$$e(t) = x_a(t) - x_d(t) \quad (13)$$

where $q_d(t)$ is the desired trajectory and $q_a(t)$ is the actual trajectory being followed by the manipulator. The state space form of dynamic equation is given by (14)

$$\frac{d}{dt}\begin{bmatrix} e \\ \dot{e} \end{bmatrix} = \begin{bmatrix} 0 & I \\ 0 & 0 \end{bmatrix}\begin{bmatrix} e \\ \dot{e} \end{bmatrix} + \begin{bmatrix} 0 \\ I \end{bmatrix} U \quad (14)$$

To achieve desired trajectory, control law U is based on PID and is given by (15)

$$U = -K_v\dot{e} - K_p e - K_i \int e\, dt \quad (15)$$

The joint torque τ is related with the control input Uas

$$\tau = M(\ddot{x_d} - U) + V(\dot{x}, x) + g(x) \quad (16)$$

Combining (15) and (16) results in the required torque equation

$$\tau = M\left(\ddot{x}_d - K_v\dot{e} - K_p e - K_i\int e\,dt\right) + V(\dot{x},x) + G(x) \qquad (17)$$

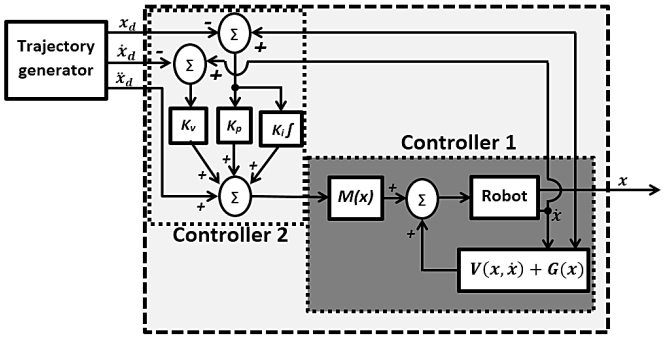

Fig. 11. CTC-PID block diagram.

The other developed control technique is SMC. It is a robust control strategy used for non-linear structure control. SMC involves two phases: Starting from a non-zero initial state, the system reaches the sliding surface, where it stays for future.

In order to design the control law via sliding mode approach, a general architecture is presented in the forthcoming study. Consider a non-linear system represented by

$$\dot{x} = f(x,t) + b(x,t)u + \Delta(x,t) \qquad (18)$$

where $x\epsilon\, R^n$ is the measurable states vector and $u\epsilon R$ is the applied control input to the system. The known terms $f(x,t)$ and $b(x,t)$ are sufficiently smooth vector fields.

The term $\Delta(x,t)$ is a matched uncertainties vector and is assumed to be norm bounded i.e.,$\Delta(x,t) = b(x,t)\delta(t)$, where $\delta(t)$ is known and bounded by a positive constant i.e., $\|\delta(t)\| \le K^*$.

Furthermore, assuming the system in (18) is in canonical form, the control objective is to regulate the system states to zero even in the presence of uncertainties. This can be done by defining a sliding manifold as follows

$$s = Cx(t) \qquad (19)$$

where C is a row vector of compatible dimension to the states vector, whose entries are chosen positive such that the manifold defined in (19) becomes Hurwitz monic polynomial. In sliding mode, the main objective is to keep $\mathrm{s} = 0$ via the control law. The control law is designed in such a way that it meets this requirement after sometimet_s. The satisfaction of $\mathrm{s} = 0$ provides order reduction which results in the insensitivity of the closed loop system to the matched disturbances. In other words, the robustness against uncertainties increases via the order reduction and the system evolves with $n-1$ states in sliding mode. The control law designed via sliding mode appears as follows

$$u = u_{eq} + u_{dis} \qquad (20)$$

where u_{eq} represents the equivalent control input (Utkin, 1992) and u_{dis} is a discontinuous control term. The first component on the right hand side of (20) is designed by posing $\dot{s} = 0$ along the dynamics of (18) while assuming that $\Delta(x,t) = 0$. Consequently,

$$u_{eq} = b^{-1}(x,t)(-f(x,t)) \qquad (21)$$

This control law is able to keep $\dot{s} = 0$ but one may have $\mathrm{s} \neq 0$ which dictates that sliding mode is not enforced. Therefore, u_{dis} in (20) is designed in such a way that it rejects/nullifies the effect of the disturbance term and maintains $s = 0$. This component can be designed by defining a Lyapunov function of the following form

$$v = 0.5s^2$$

The time derivative of this function along (18) becomes

$$\dot{v} = s\dot{s} = s\left(\frac{\partial s}{\partial x}(f(x,t) + b(x,t)u + \Delta(x,t))\right) \qquad (22)$$

Substituting (20) and (21), (22) takes the form

$$\dot{v} = s(b(x,t)u_{dis} + \Delta(x,t))$$

Using norm bounded assumption, the above expression reduces to

$$\dot{v} = b(x,t)s(u_{dis} + \delta(t))$$

Considering $u_{dis} = -Ksign(s)$, the above expression becomes

$$\dot{v} = b(x,t)(-sKsign(s) + s\delta(t))$$

or

$$\dot{v} \le -||b(x,t)|||s|(K - |\delta(t)|)$$

Therefore,

$$\dot{v} \le -\mu|s| = -\sqrt{2}\mu v^{\frac{1}{2}} \qquad (23)$$

provided that $K - |\delta(t)| \ge \mu > 0$. The differential inequality in (23) confirms that sliding mode takes place in finite time t_s even in the presence of uncertainties.This means that $\mathrm{s} = 0$ holds after $t_s \le \sqrt{2}\mu^{-1}v_0^{\frac{1}{2}}$, where v_0 represents the energy of the system at timet_0.

Consequently, the closed loop dynamics can be written as

$$\begin{bmatrix}\dot{x}_1\\ \dot{x}_2\\ \vdots\\ \dot{x}_{n-1}\end{bmatrix} = \begin{bmatrix}0 & 1 & 0 & \dots & 0\\ 0 & 0 & 1 & \dots & 0\\ \vdots & \dots & \ddots & 1 & 0\\ -\mathrm{c}_1 & -\mathrm{c}_2 & \dots & \ddots & -\mathrm{c}_{n-1}\end{bmatrix}\begin{bmatrix}x_1\\ x_2\\ \vdots\\ x_{n-1}\end{bmatrix} \qquad (24)$$

Since, the constants c_i(entries of C in (19)) are chosen positive, therefore, the poles of this closed loop system is in the left half plane. Thus, $x \to 0$ as $t \to \infty$ and the system in (24) is unaffected by the uncertainties is satisfying the invariance property of sliding mode control.

In the present research, the dynamics of each link is a second order system (i.e. *n*=2). Therefore, (12) can be re-written alternatively as (25)

$$\begin{aligned}\dot{x}_1 &= x_2\\ \dot{x}_2 &= M^{-1}(x_1)\big(-V(x_1,x_2) - G(x_1)\big) + M^{-1}(x_1)U\end{aligned} \qquad (25)$$

Now, the control objective is that the system is able to follow a desired trajectory x_d. This task can be fulfilled by defining a sliding manifold of the error variables $e = x - x_d$ and $\dot{e} = \dot{x} - \dot{x}_d$ in the forthcoming form

$$s(e,\dot{e}) = \dot{e} + \lambda e \qquad (26)$$

Following the design strategy, the final expression of the controlled input *U* becomes

$$U = M(x_1)[M^{-1}(x_1)\big(V(x_1, x_2) + G(x_1)\big) + \ddot{x}_d - \lambda(\dot{x} - x_d)] - Ksign(s) \quad (27)$$

This input U will enforce sliding mode against the switching manifold $S(e, \dot{e})$. The system dynamics will be maintained at this manifold for all future time$t \geq t_s$. Consequently, the closed loop system $\dot{e} + \lambda e$ =0 will remain valid and e will approach to zero asymptotically. The convergence of e to zero, in other words, ensures that the system follows the desired trajectory x_d.

Figure 12 shows implementation of SMC for the robotic arm.

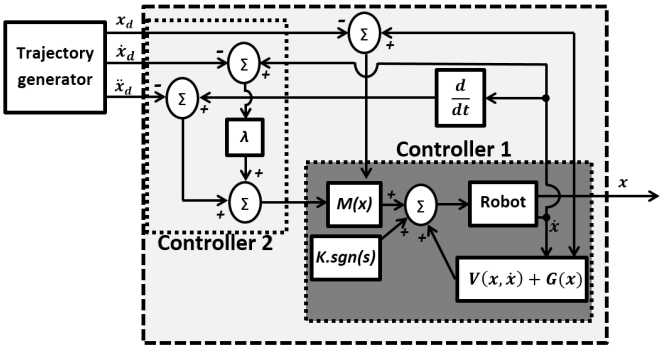

Fig. 12. SMC block diagram.

5. RESULTS AND DISCUSSION

Based on the derived models and tuned gains, both CTC-PID and SMC have been simulated. The model has been subjected to various reference inputs including step, impulse, ramp and sinusoidal etc. to investigate the dynamic characteristics and to analyze the control scheme. The capability of control to track these inputs has been verified in simulations. For each reference input, response corresponding to each robotic joint has been displayed. Figure 13(a-d) demonstrates step, impulse, ramp and sinusoidal response of elbow, base, wrist and shoulder joints, respectively.

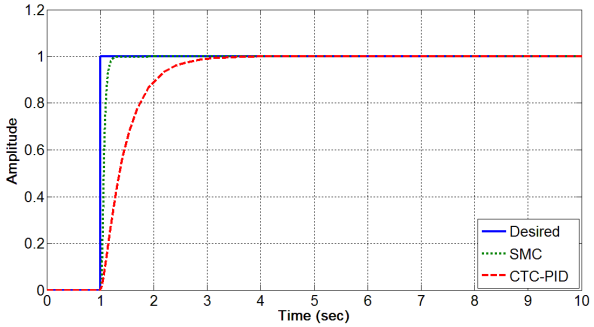

(a)

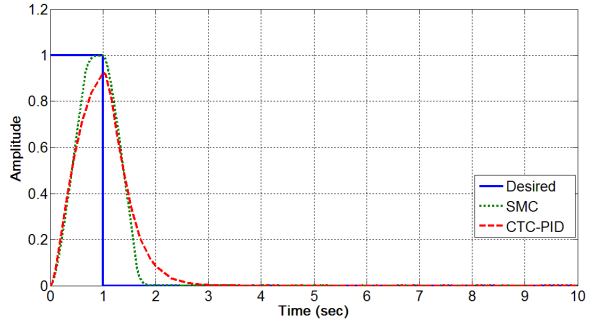

(b)

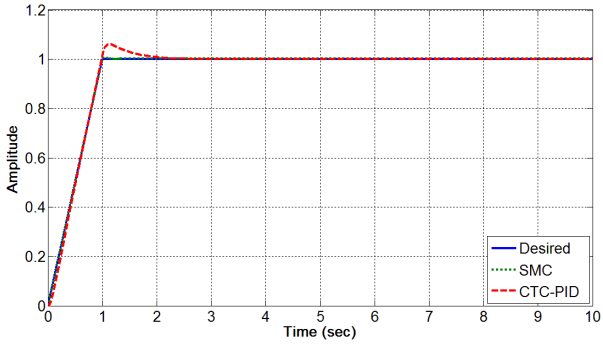

(c)

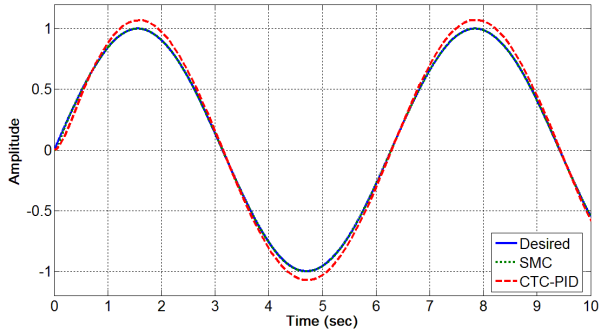

(d)

Fig. 13. Performance of CTC-PID and SMC demonstrated by (a) Step response at Elbow (b) Impulse response at Base (c) Ramp response at Wrist (d) Sinusoidal response at shoulder.

Considering step response (Fig. 13a), the performance comparison of CTC-PID and SMC is listed in Table 4. The results of SMC are far better that that of CTC-PID.

Table 4. Performance comparison of CTC-PID and SMC.

Parameter	Symbol	Control Strategy	
		CTC-PID	SMC
Rise time	t_r(sec)	1.95	1.13
Peak time	t_p(sec)	3.9	1.32
Settling time	t_s(sec)	4.1	1.32
Overshoot	%OS	1.12	0

Comparing impulse response of base joint (Fig. 13b) via CTC-PID and SMC, it is clear that SMC is responding quite sharply as compared to CTC-PID. It is also evident that the CTC-PID results do not reach the desired point in the beginning. In addition, when wrist is subjected to ramp input (Fig. 13c), overshoot is observed in case of CTC-PID. Furthermore, the sinusoidal response of shoulder joint using CTC-PID and SMC is depicted in Fig 13d. The SMC response is very close to the desired one. However, there exists steady state error in case of CTC-PID. Thus, SMC outshines CTC in all these aspects.

In this study, robustness analysis is also presented for both the techniques in the presence of a bounded time varying matched disturbance. Figure 14a illustrates the disturbance being added on the control input channel in both cases. The tracking performance of the presented techniques is shown in Figure 14b. Once again, it is clear that SMC shows insensitivity to the added disturbance while the response of

CTC-PID is deteriorated with addition of the disturbance. In nutshell, SMC is a good candidate for robotic systems.

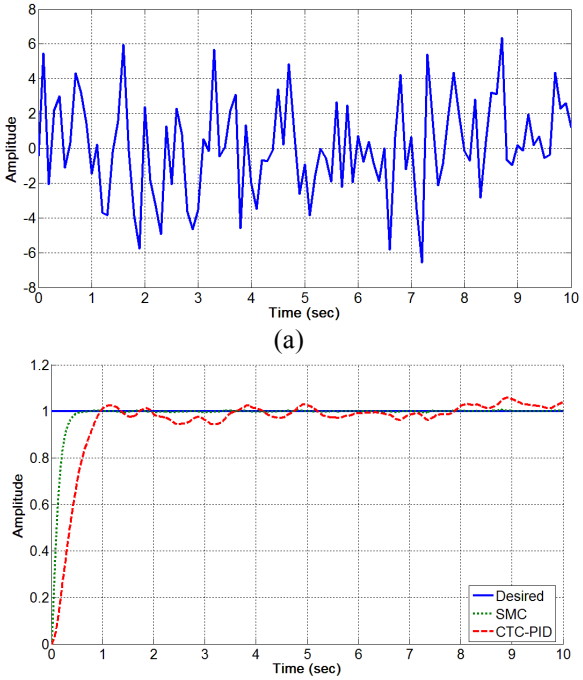

Fig. 14. Disturbance rejection: (a) Bounded matched disturbance, (b). Tracking performance of CTC-PID and SMC

6. CONCLUSION

An articulated based novel platform for autonomous applications has been mentioned in this research. The platform finds its potential applications in educational, academic, research and industrial sectors. Exploiting the open hardware and software architectures of the custom-developed prototype, the present research presents design and performance comparison of CTC and SMC strategies. Given various input trajectories to characterize the response, simulation results demonstrate that SMC has superior performance in terms of transient parameters. In Steady state, both CTC and SMC manage to converge to the desired output though the later attains steady value faster.

The digitization of the simulated control techniques is in consideration in order to implement these control approaches on the physical system. Moreover, availability of on-board camera and Force Sensing Resistor (FSR) in the gripper permits implementation of more sophisticated control techniques by combining image processing and force feedback. In an attempt to conduct multi-disciplinary research, another planned project is to control the robotic arm based on Brain Controlled Human Robot Interface (HRI) mentioned in (Khurram et al., 2012).

ACKNOWLEDGEMENTS:

We would like to acknowledge COMSATS Institute of Information Technology, Pakistan for providing funding to conduct this research. Special thanks to Dr. Muhammad Fasih Uddin Butt, Director - Modelling and Simulation Lab. for providing resources and environment to facilitate write-up of this paper. Warm regards to Mr. Ahmad Mahmood Tahir for proofreading the manuscript.

REFERENCES

Antonio, Y., Victor, S., and Javier, M.V. (2011). Global asymptotic stability of the classical PID controller by considering saturation effects in industrial robots. *International Journal of Advance Robotic Systems*, vol. 8, pp.34-42.

Birla, N., and Swarup, A. (2013). Design of adaptive preview control. *Journal of Control Engineering and Applied Informatics* (CEAI), vol.15 (1), pp. 71-78.

Chia-Shang, L., and Peng H. (2000). Disturbance observer based tracking control. *Journal of Dynamic Systems, Measurement, and Control*, vol. 122, pp. 332-335.

Craig, J.J. (2005). *Introduction to Robotics: Mechanics and Control.* Prentice Hall, New Jersey.

Dimitri, M., and Anwari, S. (2009). Robust adaptive control for robotic manipulator based on chattering free variable structure system. In: Proc. *IEEE International Conference on Electrical Engineering and Informatics.* pp. 247-252.

Duy, N.T., Matthias, S., and Jan, P. (2008). Computed torque control with nonparametric regression models. In: Proc. *American Control Conference*, pp. 212-217.

Farzin, P., Mohammad, H.Y., Mohammad, S., Ebrahim, M., and Ali, H. (2012a). PUMA-560 robot manipulator position computed torque control methods using Matlab/Simulink and their integration into graduate nonlinear control and Matlab courses. *International Journal of Robotics and Automation (IJRA)*, vol. 3, pp. 167-191.

Farzin, P., Sara, E., Zahra, H., Forouzan, S., and Mina, M. (2012b). PUMA-560 robot manipulator position sliding mode control methods using Matlab/Simulink and their integration into graduate/undergraduate nonlinear control, robotics and Matlab courses. *International Journal of Robotic and Automation, (IJRA)*, vol.6, pp. 106-150.

Fayaz, M.K., Raza, U.I., and Iqbal, J. (2012). Control strategies for robotic manipulators. In: Proc. *IEEE International Conference on Robotics and Artificial Intelligence (ICRAI)*, pp. 26-33.

Fu, K.S., Gonzalez, R.S., and Lee, C.S.G. (2008). *Robotics Control, Sensing, Vision and Applications*, Tata McGraw-Hill Publishing.

Groover, M.P., Weiss, M., Nagel, R.N., and Odrey, N.G. (2008). *Industrial Robotics – Technology, Programming and Applications*, Tata McGraw-Hill Publishing.

Hiroyuki, K., Toshiyuki, M., Ryuichi, S., and Masayuki, F. (2011). Passivity-based control for 2-DOF robot manipulators with antagonistic bi-articular muscles. In: Proc. *IEEE International Conference on Control Applications (CCA)*, pp. 1451–1456

Iqbal, J., Tsagarakis, N.G., Fiorilla, A.E., and Caldwell, D.G. (2010). A portable rehabilitation device for the hand. In: Proc. *32nd Annual IEEE International Conference of Engineering in Medicine and Biology Society (EMBS)*, Buenos Aires, Argentina, pp. 3694-3697.

Iqbal, J., Tsagarakis, N.G., and Caldwell, D.G. (2011). A multi-DOF robotic exoskeleton interface for hand motion assistance, In: Proc. *33rd Annual IEEE International Conference of Engineering in Medicine and Biology Society (EMBS)*, Boston, US, pp. 1575-1678.

Iqbal, J., Raza U.I., and Khan, H. (2012). Modeling and analysis of a 6 DOF robotic arm manipulator. *Canadian Journal on Electrical and Electronics Engineering* (ISSN: 1923-0540), vol. 3(6), pp. 300-306.

Iqbal, J., Nabi, R., Khan, A.A., and Khan, H. (2013).A novel track-drive mobile robotic framework for conducting projects on robotics and control systems. *Life Sci Journal* (ISSN 1097-8135) vol. 10(3), pp. 130-137.

Jing, Z., Xin, G., and En, L. (2011). An adaptive variable structure controller for robotic manipulators. In: Proc. *6th International Forum on Strategic Technology (IFOST),* vol.1, pp. 351 – 355.

Jingmei, Z., Haiyang, H., and Bo, K. (2012). Studies of adaptive control methods based on VSC for trajectory tracking of robotic manipulators. In: Proc. *International Conference on Robotics and Biomimetics (ROBIO)*, pp. 429 – 434.

Khoi, B.N., and Robert, M. (2005). Passivity-based control of robot manipulators subject to constraints. In: Proc. *Australasian Conference on Robotics and Automation (ACRA),* pp. 1-7.

Khurram, N., Iqbal, J., and Habib, U.R. (2012). Brain controlled human robot interface. In: Proc. *IEEE International Conference on Robotics and Artificial Intelligence (ICRAI)*, pp. 55-60.

Nawal, A., and Lamir, S. (2011). Passivity based adaptive control of robotic manipulators electrically controlled. *International Journal of Advanced Science and Technology*, vol. 34, pp. 45-54.

Ouyang, P.R., Acob, J., and Pano, V. (2014). PD with sliding mode control for trajectory tracking of robotic system, Robot Cim-Int Manuf, vol. 30(2), pp. 189-200.

Raza, U.I., Iqbal, J., Sarah, M., Aayman, K., and Sana, K. (2012). An autonomous image-guided robotic system simulating industrial applications. In: Proc. *IEEE International Conference on System of Systems Engineering (SOSE)*, Italy, pp. 344-349.

Saha, S.K. (2008). *Introduction to Robotics*, McGraw-Hill Education.

Suolin, D., Lanping, C., Zhenghua, M., and Guirong, L. (2010). Variable structure control with feed forward compensator for robot manipulators subject to load uncertainties. In: Proc. *IEEE International Conference on Control, Automation, Robotics and Vision (ICARCV)*, pp. 2367-2372.

Utkin, V. I. (1992). *Sliding Modes in Control Optimization*, Springer, Berlin, Germany.

Wen-Hua, C., Donald, J.B., Peter, J.G, and John, O.R. (2000). A nonlinear disturbance observer for robotic manipulators. *IEEE Transactions on Industrial Electronics*, vol. 47, pp. 932 – 938.

APPENDIX A. DYNAMIC MODEL

Let m_1, m_2, m_3 and m_4 represent the mass of each link while l_1, l_2, l_3 and l_4 represent their lengths. a,b,c,d,e,k are constants whose values have been computed based on the Inertia matrices of each link. $a=0.0026m^2$, $b=0.0024m^2$, $c=0.0059m^2$, $d=0.0044m^2$, $e=0.0024m^2$, $k=0.0020m^2$.

$$M_\omega = \begin{bmatrix} m_{11} & 0 & 0 & 0 \\ 0 & m_{22} & m_{23} & m_{24} \\ 0 & m_{32} & m_{33} & m_{34} \\ 0 & m_{42} & m_{43} & m_{44} \end{bmatrix}$$

$$\mathbf{m_{11}} = am_1 + (c+b)(m_2+m_3) + em_4$$

$$\mathbf{m_{22}} = d(m_2+m_3) + km_4$$

$$\mathbf{m_{23}, m_{32}} = dm_3 + km_4$$

$$\mathbf{m_{24}, m_{42}} = km_4$$

$$\mathbf{m_{33}} = dm_3 + km_4$$

$$\mathbf{m_{34}, m_{43}} = km_4$$

$$\mathbf{m_{44}} = km_4$$

$$M_v = \begin{bmatrix} m_{11} & 0 & 0 & 0 \\ 0 & m_{22} & m_{23} & m_{24} \\ 0 & m_{32} & m_{33} & m_{34} \\ 0 & m_{42} & m_{43} & m_{44} \end{bmatrix}$$

$$\mathbf{m_{11}} = (m_2+m_3+m_4)c_2{}^2 l_2{}^2 + (m_3+m_4)(l_3{}^2 c_{23}{}^2 + 2l_2 l_3 c_2 c_{23}) + m_4(l_4{}^2 s_{234}{}^2 - 2l_2 l_4 c_2 s_{234} - 2l_3 l_4 c_{23} s_{234})$$

$$\mathbf{m_{22}} = (m_2+m_3+m_4)l_2{}^2 + (m_3+m_4)(l_3{}^2 + 2l_2 l_3 c_3) + m_4(l_4{}^2 - 2l_2 l_4 s_{34} - 2l_3 l_4 s_4)$$

$$\mathbf{m_{23}, m_{32}} = (m_3+m_4)(l_3{}^2 + l_2 l_3 c_3) + m_4(l_4{}^2 - l_2 l_4 s_{34} - 2l_3 l_4 s_4)$$

$$\mathbf{m_{24}, m_{42}} = m_4(l_4{}^2 - l_2 l_4 s_{34})$$

$$\mathbf{m_{33}} = (m_3+m_4)l_3{}^2 + m_4(l_4{}^2 - 2l_3 l_4 s_4)$$

$$\mathbf{m_{34}, m_{43}} = m_4(l_4{}^2 - l_3 l_4 s_4)$$

$$\mathbf{m_{44}} = m_4 l_4{}^2$$

$$V = \begin{bmatrix} v_1 \\ v_2 \\ v_3 \\ v_4 \end{bmatrix}$$

$$\mathbf{v_1} = (m_2+m_3+m_4)\left(-2c_2 s_2 \dot{\theta_1}\dot{\theta_2} l_2{}^2\right) + (m_3+m_4)\left(\dot{\theta_1}\left(-2l_3{}^2 s_{23} c_{23}(\dot{\theta_2}+\dot{\theta_3}) + 2l_2 l_3\left(-c_2 s_{23}(\dot{\theta_2}+\dot{\theta_3}) - c_2 s_{23}\dot{\theta_2}\right)\right)\right) + m_4\left(\dot{\theta_1}\left(-2l_4{}^2 s_{234} c_{234}(\dot{\theta_2}+\dot{\theta_3}+\dot{\theta_4}) - 2l_2 l_4\left(c_2 c_{234}(\dot{\theta_2}+\dot{\theta_3}+\dot{\theta_4}) - s_2 s_{234}\dot{\theta_2}\right) - 2l_3 l_4\left(c_{23} c_{234}(\dot{\theta_2}+\dot{\theta_3}+\dot{\theta_4}) - s_{23} s_{234}(\dot{\theta_2}+\dot{\theta_3})\right)\right)\right)$$

$$\mathbf{v_2} = (m_2+m_3+m_4)\left(c_2 s_2 \dot{\theta_1}{}^2 l_2{}^2\right) + (m_3+m_4)(2l_3{}^2 s_{23} c_{23}\dot{\theta_1}{}^2 + l_2 l_3\left(-s_3\dot{\theta_3}(2\dot{\theta_2}+\dot{\theta_3}) - (c_2 s_{23}+s_2 c_{23})\dot{\theta_1}{}^2\right)) + m_4(-l_4{}^2 s_{234} c_{234}\dot{\theta_1}{}^2 + l_2 l_4\left(c_{34}(\dot{\theta_3}+\dot{\theta_4})(-2\dot{\theta_2}-\dot{\theta_3}-\dot{\theta_4}) + (c_2 c_{234}-s_2 s_{234})\dot{\theta_1}{}^2\right) + l_3 l_4\left(c_{34}\dot{\theta_4}(-2\dot{\theta_2}-2\dot{\theta_3}) + (c_{23} c_{234}-s_{23} s_{234})\dot{\theta_1}{}^2\right))$$

$$\mathbf{v_3} = (m_3+m_4)(l_3{}^2 s_{23} c_{23}\dot{\theta_1}{}^2 + l_2 l_3\left(-s_3\dot{\theta_3}\dot{\theta_2} + c_2 s_{23}\dot{\theta_1}{}^2\right)) + m_4(-l_4{}^2 s_{234} c_{234}\dot{\theta_1}{}^2 - l_2 l_4\left(c_{34}\dot{\theta_2}(\dot{\theta_3}+\dot{\theta_4}) + c_{34}\dot{\theta_2}(\dot{\theta_2}+\dot{\theta_3}+\dot{\theta_4}) + c_2 c_{234}\dot{\theta_1}{}^2\right) + l_3 l_4\left(c_4\dot{\theta_4}(-2\dot{\theta_2}-2\dot{\theta_3}-\dot{\theta_4}) + (c_{23} c_{234}-s_{23} s_{234})\dot{\theta_1}{}^2\right))$$

$$\mathbf{v_4} = m_4(-l_4{}^2 s_{234} c_{234} \dot{\theta_1}^2 - l_2 l_4 \left(c_{34}\dot{\theta_2}(\dot{\theta_3} + \dot{\theta_4}) - c_{34}\dot{\theta_2}(\dot{\theta_2} + \dot{\theta_3} + \dot{\theta_4}) - c_2 c_{234}\dot{\theta_1}^2\right) - l_3 l_4 \left(c_4(\dot{\theta_3}\dot{\theta_4} - \dot{\theta_2}(\dot{\theta_2} + \dot{\theta_3}) - \dot{\theta_3}(\dot{\theta_2} + \dot{\theta_3} + \dot{\theta_4})) + c_{23} c_{234}\dot{\theta_1}^2\right)\right)$$

$$G = \begin{bmatrix} 0 \\ g_2 \\ g_3 \\ g_4 \end{bmatrix}$$

$\mathbf{g_2} = (m_2 + m_3 + m_4)(-c_2 l_2 g) + (m_3 + m_4)(-c_{23} l_3 g) + m_4(s_{234} l_4 g)$

$\mathbf{g_3} = (m_3 m_4)(-c_{23} l_3 g) + m_4(s_{234} l_4 g)$

$\mathbf{g_4} = m_4(s_{234} l_4 g)$